



Layered convection with an interface at a depth of 1000 km: stability and generation of slab-like downwellings

Hana Čížková*, Ctirad Matyska

Department of Geophysics, Faculty of Mathematics and Physics, Charles University, V Holešovičkách 2, 180 00 Praha 8, Czech Republic

Received 13 November 2002; received in revised form 10 November 2003; accepted 24 November 2003

Abstract

We investigate the stability of hypothetical layered convection in the mantle and the mechanisms how the downwelling structures originating in the lower layer are generated. The stability is studied by means of numerical simulations of the double-diffusive convection in a 2D spherical model with radially dependent viscosity. We demonstrate that the stability of the layering strongly depends not only on the density contrast between the layers but also on the heating mode and the viscosity profile. In the case of the classical Boussinesq model with an internally heated lower layer, the density contrast of about 4% between the compositionally different materials is needed for the layered flow to be maintained. The inclusion of the adiabatic heating/cooling in the model reduces the temperature contrast between the two layers and, thus, enhances the stability of the layering. In this case, a density contrast of 2–3% is sufficient to preserve the layered convection on a time scale of billions of years. The generation of the downwelling structures in the lower layer occurs via mechanical or thermal coupling scenarios. If the viscosity dependent on depth and average temperature at each depth is considered, the low viscosity zone develops at a boundary between the two convecting layers which suppresses mechanical coupling. Then the downwelling structures originating in the lower layer develop beneath upper layer subductions, thus resembling continuous slab-like structures observed by seismic tomography.

© 2003 Elsevier B.V. All rights reserved.

Keywords: Layered convection; Stable reservoirs; Subduction

1. Introduction

The geochemical observations of isotopic ratios are often interpreted as an evidence of the existence of stable reservoirs of primitive material in the deep mantle (Hofmann, 1997). Until recently, the lower mantle was often considered to be such a reservoir and the 660 km discontinuity was supposed to be its upper boundary. This view was challenged in the mid-nineties when

the high-resolution seismic tomography revealed lithospheric slabs continuously passing to the lower mantle (e.g., van der Hilst et al., 1997; Bijwaard et al., 1998). Kellogg et al. (1999) proposed a new, deeper location of the primitive mantle by shifting its upper boundary to a depth of 1600 km. They have shown that the primitive material below this depth remains unmixed with the rest of the mantle provided that its density is by some 4% higher than the density of the overlying depleted material. The other candidate for the location of the upper boundary of the primitive mantle is the depth of 1000 km (for the review see, e.g. Anderson, 2001). This location seems to be compatible with some geochemical data (Turcotte et al., 2001; Anderson, 2002)

* Corresponding author. Tel.: +420-2-2191-2544;
fax: +420-2-2191-2555.
E-mail addresses: hana.cizkova@mff.cuni.cz (H. Čížková),
ctirad.matyska@mff.cuni.cz (C. Matyska).

as well as with seismic observations (Kawakatsu and Niu, 1994; Montagner and Guillot, 2000) and geodynamic modeling (Wen and Anderson, 1997). On the contrary, some other authors consider the concept of a primitive mantle untenable (e.g. Coltice and Ricard, 1999) and they propose such explanations of the geochemical record that do not require the existence of a layer of primitive material (for the review, see Tackley, 2000). This view is not necessarily in contradiction with the concept of layered or partially layered convection. The layering in these models is rather a consequence of active chemical mixing and segregation processes (Mambole and Fleitout, *in press*) than of the existence of a primitive mantle material.

In the present study we will investigate the stability of layered convection with an assumed interface at 1000 km. This depth was chosen in accordance with the geochemical arguments summarized by Anderson (2002). The layered convection is stable if the density contrast between the layers due to the difference in chemical composition is sufficiently high to compensate the thermal buoyancy associated with a temperature increase across the thermal boundary layer (Davaille, 1999). The usual density contrast considered in the layered convection simulations is around 4% (e.g., Kellogg et al., 1999). This value seems somewhat high from the seismological point of view since there is no seismic indication for such a high density increase at a depth of 1000 or 1600 km.

The aim of our study is to find the smallest density contrast which is able to maintain the layered convection stable. The density contrast considered between the upper and lower layer (not necessarily linked to depleted/primitive mantle) ranges between 1 and 5%. Besides the effect of the density contrast we will also investigate the role of different heating modes (bottom, internal) and the effect of adiabatic heating/cooling which may influence the magnitude of the thermal buoyancy.

Since there are seismic tomographic images of the slabs continuously passing through the mantle to the depths of at least 1600 km and sometimes even to the core–mantle boundary, we concentrate here also on the question how the downwellings are generated in the lower mantle and whether the seemingly continuous slab-like structures could be generated via thermal coupling mechanism (Čížková et al., 1999).

2. Method

We consider incompressible Newtonian flow in an axisymmetric mantle heated both from below and internally. The field approach is used to describe the convection in a system with two compositionally distinct layers. In Boussinesq approximation the double-diffusive convection is described by the following set of equations describing the conservation of mass:

$$\nabla \cdot \mathbf{v} = 0, \quad (1)$$

conservation of momentum

$$\nabla \cdot \boldsymbol{\tau} + \varrho \mathbf{g} = 0 \quad (2)$$

and conservation of energy

$$\frac{\partial T}{\partial t} = -\mathbf{v} \cdot \nabla T + \nabla \cdot (\kappa \nabla T) + \frac{Q_v}{\varrho C_p}. \quad (3)$$

In Eqs. (1)–(3), ϱ denotes the density, \mathbf{v} the velocity, t the time, $\boldsymbol{\tau}$ represents the stress tensor, \mathbf{g} the gravity acceleration, T the temperature, C_p the specific heat at constant pressure and κ the thermal diffusivity and Q_v the internal heating rate. Advection of composition follows the equation similar to (3):

$$\frac{\partial C}{\partial t} = -\mathbf{v} \cdot \nabla C + \kappa_C \nabla^2 C, \quad (4)$$

where C is composition (concentration of a dense material) and κ_C is compositional diffusivity. Constitutive law for Newtonian incompressible fluid reads

$$\boldsymbol{\tau} = -p\mathbf{I} + 2\eta\dot{\boldsymbol{\epsilon}}. \quad (5)$$

Here p is the pressure, \mathbf{I} the identity matrix, η the viscosity and $\dot{\boldsymbol{\epsilon}}$ the strain-rate tensor. State equation describing changes in density due to thermal and compositional differences is

$$\varrho = \varrho_0(1 - \alpha(T - T_0)) + \beta(C - C_0) \quad (6)$$

with ϱ_0 being the reference density at $T = T_0$ and $C = C_0$, α the thermal expansivity and β its compositional counterpart.

The calculations have been carried out with the semi-spectral code combining spherical harmonics laterally and finite differences with radius (Čížková and Čadek, 1997). The resolution of the model is 10–30 km in radius and about 35 km laterally. In some of our

model calculations adiabatic heating effect was included (term $-g\alpha T v_r / C_p$, where v_r is the radial component of velocity, added on the right-hand side of Eq. (3)). In these calculations viscous dissipation term was not included in order to avoid additional computational costs.

The initial state is represented by two chemically distinct layers with the different density. The initial chemical concentration is set to 1 in the bottom layer, stretching from the 1000 km depth down to the CMB, and to 0 in the upper layer. The initial temperature distribution corresponds to a fully layered flow, i.e., to a state in statistical equilibrium obtained by simulating the thermal convection in a model with non-deforming impermeable boundary at a depth of 1000 km. Such initial temperature distribution is calculated for each studied model. After reaching this state, at time $t = 0$, the impermeable boundary is removed and the subsequent evolution of the system is simulated by solving equations of the double-diffusive convection with the Lewis number of 100. The goal of this study is to find such model parameters that allow the original layered flow pattern to be preserved. The system of convection will be considered stable if the both reservoirs remain continuous and the topography of the interface does

not exceed a few hundred kilometers on a time scale of billion of years.

We consider three basic models of mantle viscosity in our calculations: model A, characterized by a constant viscosity, model B in which the viscosity increases with depth (Fig. 1, solid line), and model C where the viscosity depends on pressure and average temperature. Model B roughly corresponds to the viscosity profile inferred from the geoid by Ricard and Wuming (1991). The existence of a viscosity hill in the lower mantle was also recently reported by Mitrović and Forte (2002). The pressure (depth) and temperature dependence of viscosity in the model C is prescribed by the formula:

$$\eta = \eta_0 \exp\left(\frac{a}{T} + b\frac{z}{T}\right), \quad (7)$$

where T is the average temperature at a depth z . The parameters in Eq. (7) were chosen as follows: $\eta_0 = 4.8 \times 10^{18}$ Pa s, $a = 2.4 \times 10^3$ K, $b = 4.2 \times 10^{-3}$ K m $^{-1}$. In some of the runs, an 80 km thick lithosphere is added to a constant viscosity model. The viscosity of the lithosphere is 100 times higher than the mantle viscosity (model A_L). The tested values of the density contrast between the two layers range from 1 to 5%.

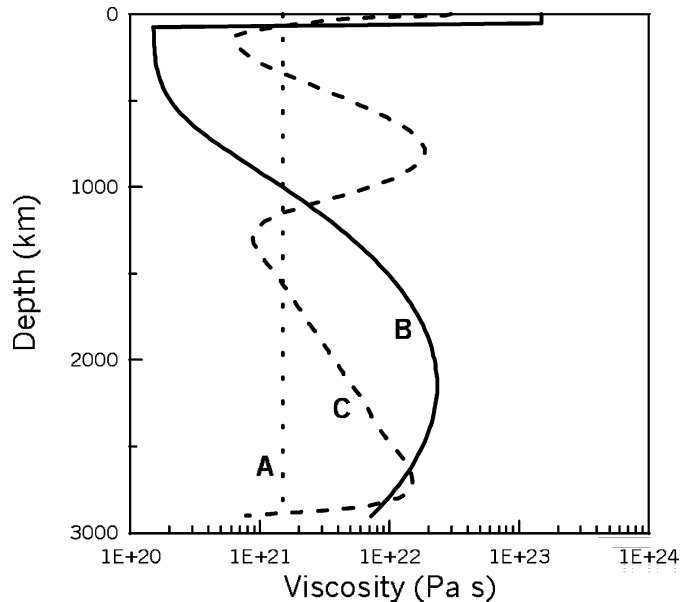


Fig. 1. Viscosity profiles used in this study. A detailed description of the viscosity models A, B and C can be found in Section 2. In the case of model C, the viscosity profile corresponding to the initial temperature distribution is plotted.

The other parameters of the model are constant. The Rayleigh number is defined as

$$Ra = \frac{\rho_0 \alpha g \Delta T d^3}{\kappa \eta}, \quad (8)$$

where ΔT is temperature difference between the upper and the lower boundary of the mantle, d the depth of the mantle and η a volume average viscosity of the mantle. Ra is 10^7 for the model A while the model B is characterized by a Rayleigh number of 1.3×10^6 . In the model C where the viscosity depends on temperature and pressure, the average Rayleigh number slightly varies with time around the value of 2×10^6 . The temperature at the core–mantle boundary is 2900 K and thermal buoyancy parameter $\alpha \Delta T$ is 0.036. The radioactive heating is only considered in the lower layer. Free-slip with zero vertical velocity, constant temperature conditions and isolating concentration conditions are imposed at the surface and the core–mantle boundary.

3. Stability of layered convection

3.1. Effect of density contrast

In the first set of numerical experiments, the effect of the density contrast between the layers is tested for an isoviscous mantle model heated purely from below. The calculations are carried out in a classical Boussinesq approximation. The initial temperature distribution is plotted in Fig. 2, panel (a). In panel (b), we show the temperature and concentration obtained for a density contrast of 1% after 20 Myr of evolution. Despite the fact that the time interval after removing the blocking impermeable interface is very short, the material of the lower layer has already reached the surface and the original lower reservoir is destroyed. If the density contrast is 2% (Fig. 2(c)), the layering is much more stable. After 200 Myr, the lower reservoir still exists but it is strongly deformed (Fig. 2(d)). The density contrast of 3% finally results in a stable layering (Fig. 2(e)).

3.2. Effect of internal heating

In the second set of experiments we concentrate on the density contrast of 2% which seems to be criti-

cal for the transition from the layered to whole mantle convection. We use the same model as in the experiments described above but we add the internal heating in the lower layer, which follows the idea of Kellogg et al. (1999). The applied density of internal heat sources ($3 \times 10^{-8} \text{ W/m}^3$) corresponds to a bulk Earth material about 1–1.5 billion years (Schmus, 1995). It accounts for approximately 1/4 to 1/3 of the total surface heat flux in our models. The results are summarized in Fig. 2(f) and (g). Fig. 2(f) shows the initial temperature distribution obtained in the model with both bottom and internal heating. Since the internal heat sources are only located in the lower layer, the average temperature in this layer is higher than in the case of the mantle heated only from below (cf. Fig. 2(a)). The situation reached after 50 Myr evolution from the initial state is illustrated in Fig. 2(g). Comparison of panels (c) and (g) clearly shows that the addition of the internal heating decreases the stability of the layering. Apparently, the reason of the distinct behavior of these two models is the difference in the temperature contrast across the mid-mantle thermal boundary layer (Fig. 3): a high temperature jump enhances the buoyancy of topographic anomalies at the interface and thus decreases the stability of the layering. The internal heating in the lower layer results in a too high temperature difference between the layers. To obtain a stable layered convection in a model with 2% density contrast we need to decrease this temperature difference.

3.3. Effect of a stiff lithosphere and adiabatic heating

We test two effects which can suppress the temperature difference between the upper and lower layer. First, we impose a high-viscosity lid on the top of our model. Such a lid stretches the temperature jump over the upper thermal boundary layer and thus decreases the jump over the mid-mantle boundary layer (Fig. 3). Since the model with a stiff lithosphere shows basically no slip at the surface, it can be considered as an end-member case of mantle flow opposite to the model with a free-slip boundary we have used above. The effect of a stiff lithosphere on the stability of the layered convection is illustrated in Fig. 2(h). Although the presence of the lithosphere significantly (approximately 10 times) delays the destruction of the lower

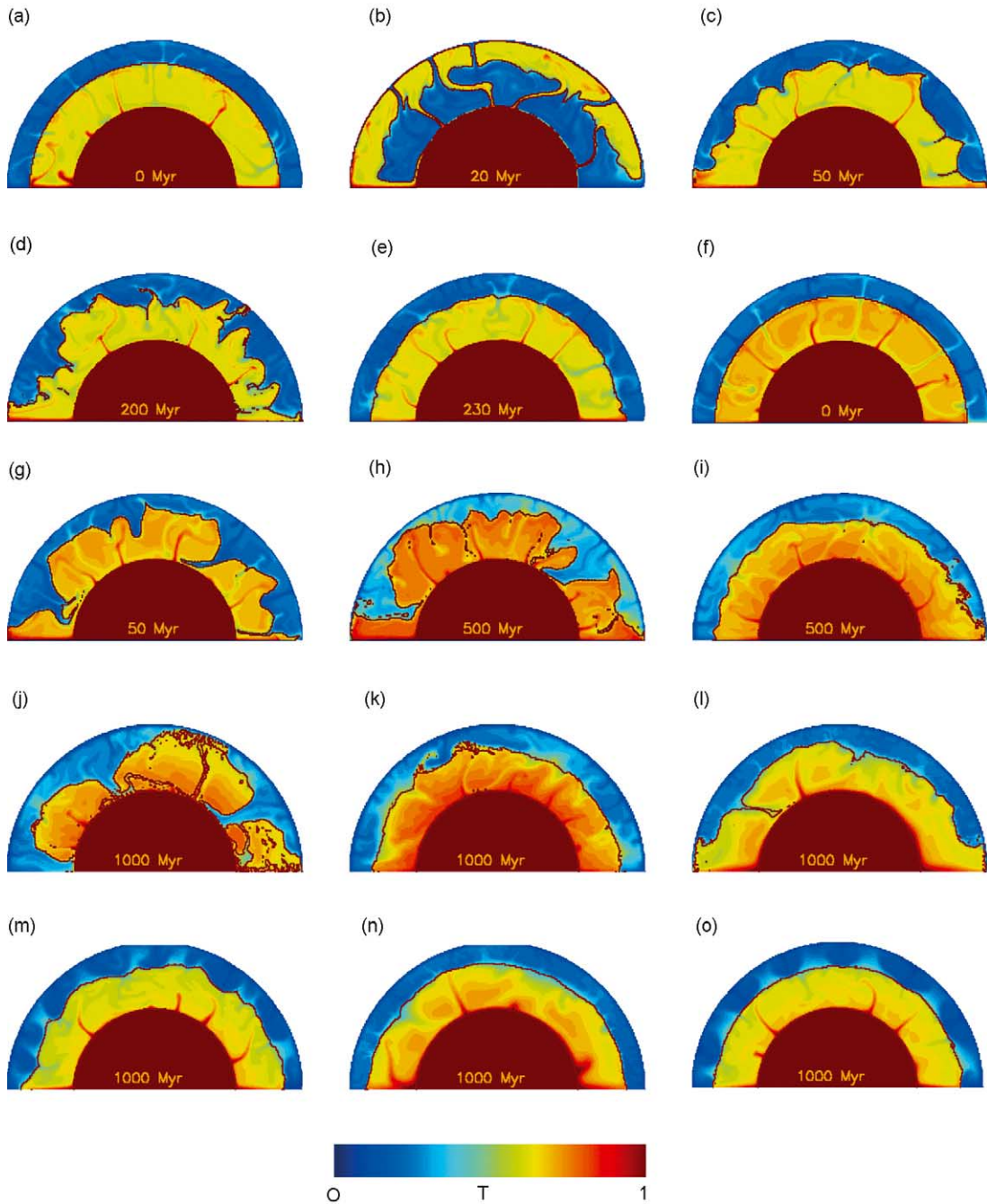


Fig. 2. Temperature and concentration fields for different model runs. The colors depict the temperature field while the dark line marks position of the boundary between the two reservoirs. Appropriate model parameters are given in Table 1.

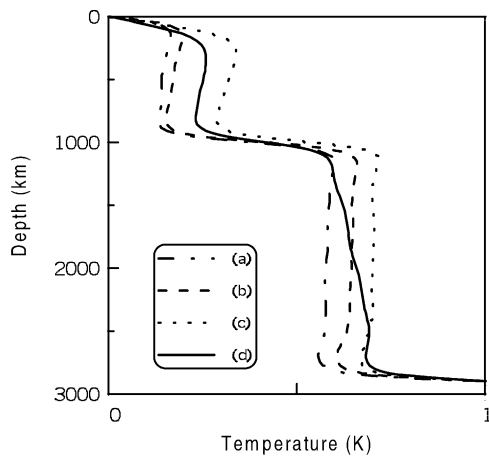


Fig. 3. Averaged geotherms of the initial temperature distribution for (a) isoviscous model heated only from below, (b) isoviscous model heated both from below and internally, (c) model with a high viscosity lid and a constant viscosity below the lithosphere heated from below and internally, and (d) the same model as (c) but with an adiabatic heating term included.

reservoir, the layered flow can hardly be preserved for more than 500 Myr.

The other effect we consider is the adiabatic heating. In the classical Boussinesq approximation where the adiabatic gradient of temperature is set to zero, the temperature outside the boundary layers is almost constant with depth. In contrast, if the adiabatic heating term is included in the thermal equation, the horizontally averaged temperature increases with depth everywhere, which reduces the temperature jumps over the boundary layers (Fig. 3). The stabilizing role of the adiabatic heating is obvious from the comparison of Fig. 2(h) and (i): After 500 Myr evolution, the model with adiabatic heating still preserves the layered style of flow (Fig. 2(i)) while the model without adiabatic heating is already in a transition from a layered to a whole-mantle flow (Fig. 2(h)). After another 500 Myr the lower layer is destroyed even in the model with the adiabatic heating (Fig. 2(j)). However, a slightly higher density contrast (3%) is already sufficient to preserve a stable layering on a time scale of billion of years (Fig. 2(k)).

3.4. Effect of viscosity stratification

In the last set of experiments, the effect of depth variations of viscosity is tested. First, we investigate

the role of a viscosity increase in the lower layer (viscosity model B, see Fig. 1). The flow in the mantle heated from both below and internally is modeled in an extended Boussinesq approximation. A high-viscosity lid is included. The results for a density contrast of 2% are illustrated in Fig. 2(l) where the thermal distribution after 1000 Myr evolution from the initial state is plotted. Compared to Fig. 2(j) (isoviscous model with a high viscosity lithosphere) the flow pattern is more stable here: a sluggish lower layer circulation apparently stabilizes the layering. The topography of the interface is rather low except for the polar regions, where ascending plumes strongly deform the boundary and the lower layer material reaches the surface.

A similar result is obtained for the model with a viscosity dependent on depth and average temperature (model C, Eq. (7)). In this case, the viscosity profile varies with time according to the changes of the average geotherm. One example, corresponding to the initial temperature distribution, is given in Fig. 1. The presence of the thermal boundary layer at a depth of 1000 km results in the viscosity profile with two maxima: one in the bottom part of the upper layer and the other in the deep lower mantle. These two maxima are separated by a broad low viscosity zone located beneath the chemical boundary. The layering in this model (Fig. 2(m)) is again more stable than in the isoviscous case and the topography of the interface is even smaller than in the case of viscosity model B (cf. Fig. 2(l)). A higher stability of the layered flow in model C may be associated with the existence of the mid-mantle low viscosity zone which mechanically decouples the convection systems in the upper and lower layers (Cserepes and Yuen, 1997) as well as with the relatively high viscosity in the lower layer (Matyska and Yuen, 2002). However, both model B and model C require a density contrast of about 3% for the amplitudes of the interface topography to be maintained below ~ 100 km (Fig. 2, panels (n) and (o)).

One of possible indications whether the model is reasonable are the geoid heights generated by the layered model. Generally, the topography of the impermeable boundary is supposed to be high and subsequently, also the geoid signal generated by layered models is expected to be too high. Here, however, we demonstrate that both surface dynamic topography and geoid amplitudes are rather low. The surface dynamic topography in model (o) (see Table 1) is

Table 1
Description of the models shown in Fig. 2

Panel	Viscosity profile	Time (Myr)	Heating mode	Adiabatic heating	Density contrast
a	A	0	Bottom	No	Initial state
b	A	20	Bottom	No	1%
c	A	50	Bottom	No	2%
d	A	200	Bottom	No	2%
e	A	230	Bottom	No	3%
f	A	0	Bottom + internal	No	Initial state
g	A	50	Bottom + internal	No	2%
h	A _L	500	Bottom + internal	No	2%
i	A _L	500	Bottom + internal	Yes	2%
j	A _L	1000	Bottom + internal	Yes	2%
k	A _L	1000	Bottom + internal	Yes	3%
l	B	1000	Bottom + internal	Yes	2%
m	C	1000	Bottom + internal	Yes	2%
n	B	1000	Bottom + internal	Yes	3%
o	C	1000	Bottom + internal	Yes	3%

shown in Fig. 4(a) for three time intervals (250, 500 and 1000 Myr). Its maximum amplitudes are about 1 km. The geoid heights calculated for the same time intervals are about 20 m (see Fig. 4(b)).

3.5. Downwellings in the lower layer

Recent seismic tomographic models seem to resolve the slab-like structures continuously passing the 660 km interface and sinking to the depths of 1600 km and some of them even to the core–mantle boundary (e.g. van der Hilst et al., 1997; Bijwaard et al., 1998). However, tomography does not trace really plate-like structures into the deep lower mantle. It seems to be clear that plates penetrate the 660 km boundary, but beneath the depth of 1000 km rather blob-like anomalies are observed. This might suggest that at about that depth there is an interface prohibiting the cold plate to sink further down. Then the fast anomalies beneath the 1000 km depth seemingly connected to the slabs in the upper third of the mantle could be explained by the thermal coupling between the separately convecting upper and lower layers.

The two separately convecting systems can be connected via mechanical coupling, thermal coupling or a combination of the two. It has been shown that in an isoviscous model (Richter and McKenzie, 1981) or in a model with a temperature-dependent viscosity (Christensen and Yuen, 1984) mechanical cou-

pling prevails and downwellings in the lower layer develop beneath upwellings in the upper layer and vice versa. This mechanical coupling can be suppressed by a strong viscosity contrast between the upper and lower layer (Cserepes et al., 1988), then the thermal coupling is enhanced. Another mechanism, which mechanically decouples upper and lower flow systems and thus enhances thermal coupling was suggested by Čížková et al. (1999). They have shown that in the model with a fixed impermeable boundary (radial flux prohibited) the existence of a low viscosity channel above or below the impermeable boundary suppresses mechanical coupling and thermally induced downwellings can be observed in the lower layer.

Since here in our model (o) (see Table 1) a low viscosity channel develops in the thermal boundary layer at a depth of around 1000 km (Fig. 1, profile C), thermally coupled slab-like structures are observed in the lower layer. Thus though there is a stable layered convection with only slightly deformed interface at a depth of 1000 km, the seemingly continuous downwellings connected with the upper layer slabs can be observed in the lower layer. Four examples of such thermally coupled slabs are shown in Fig. 5. Panel 5(a) depicts an offset structure—the lower layer downwelling (shifted by about 200 km with respect to the upper layer slab) extends almost to the core–mantle boundary. Panels 5(b)–(d) show the examples of the lower layer structures directly connected with their up-

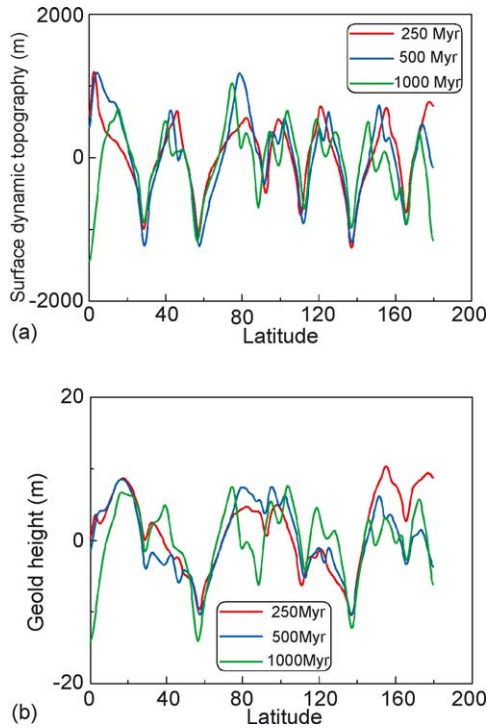


Fig. 4. (a) Surface dynamic topography as a function of latitude in the model (o) (see Table 1). Three time intervals: 250, 500 and 1000 Myr are shown. (b) Geoid heights in meters in the same time intervals.

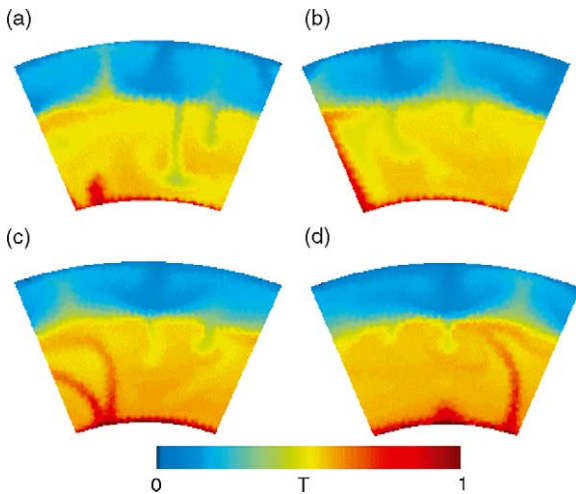


Fig. 5. Four examples of slab-like structures developed in the lower layer in model (o) (see Table 1). Plots of temperature field extend from the surface to the core–mantle boundary.

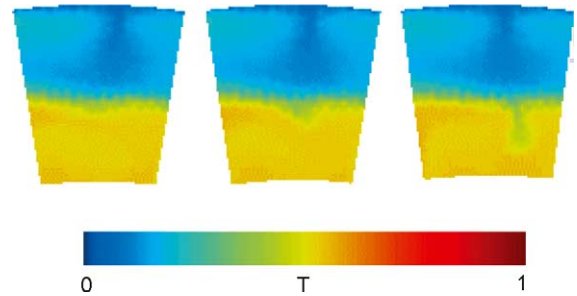


Fig. 6. Detail of the development of a slab-like structure in the lower mantle in model (o) (see Table 1). The depth extent of the plots is from the surface to the depth of 1800 km. Time difference between the snapshots is 20 Myr.

per layer counterparts. The lower layer downwellings extend to the depths of 2200, 1700 and 1500 km, respectively. Seismic velocity anomaly associated with the cold downwellings induced in the lower mantle is about 0.5–1.5% at a depth of about 1300 km (we consider a proportionality factor $\partial \ln \rho / \partial \ln v$ of 0.4).

In Fig. 6 the process of thermal induction of the downwelling in the lower layer is demonstrated on a detailed plot of a part of the mantle from the surface down to the depth of about 1800 km. Time difference between the plots is 20 Myr. In the left panel a stable cold slab in the upper layer is observed. 20 Myr later (middle panel) the downwelling in the lower layer initiates. After another 20 Myr (right panel) the slab-like structure in the lower layer extends down to a depth of about 1500 km. The development of the same structure, now in a larger space window extending down to the core–mantle boundary, is shown in Fig. 7. Here four time snapshots, again with a 20 Myr time difference are shown. The first three panels (a)–(c) are taken at the same times as the three panels in Fig. 6. In panel (a) there is a stable slab in the upper mantle, two downwellings in the lower mantle offset from the upper mantle slab by about 700 and 1300 km and a plume in the lower layer with a slightly offset continuation in the upper layer. Panel (b) shows the initiation of a new downwelling beneath the upper mantle slab while the two other downwellings are merging each other while carried away from the upper mantle slab. After another 20 Myr (panel (c)) the thermally induced slab reached the depth of 1500 km. In the last panel (d) the thermally induced downwelling is swept away by the lateral flux generated by the plume in the

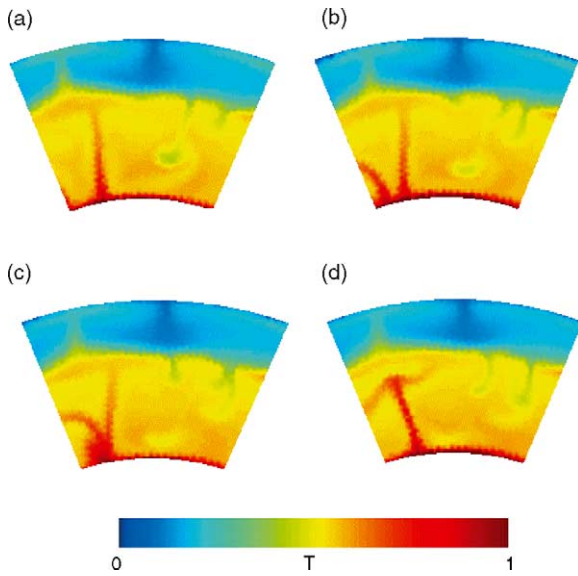


Fig. 7. Development of the same structure as in Fig. 6, but shown in a larger spatial window (extending from the surface to the CMB). Time difference between the panels is again 20 Myr. Panels (a)–(c) correspond to the three panels given in Fig. 6.

left part of the figure and thus again (as in Fig. 7(a)) an offset slab-like structure is observed.

Fig. 8 demonstrates a possibility of long-time existence of a slab-like downwellings beneath the upper layer subduction. Here six snapshots are shown with a time difference of 20 Myr. Plotted area again extends from the surface to the core–mantle boundary. A very stable plume on the left-hand side of all panels is located on the pole (e.g. one of the vertical boundaries of our axisymmetric box). In the upper layer two stable cold downwellings have evolved. The left one is connected with a downwelling in the lower layer. Panels (a) and (b) show the situation when two other cold downwellings in the lower layer, forced by a plume-push of the lower layer plumes, are approaching the one beneath the upper layer slab. In panel (c) these three downwellings merge and form one slab-like structure connected to the upper layer slab (panel (d)). Later another two downwellings appear beneath the thermal boundary layer in the mid-mantle (panel (e)) and migrate towards our ‘continuous slab’ (panel (f)). The upper layer slab attracts cold downwellings in the lower layer and an seemingly continuous slab-like structure remains stable on time scales

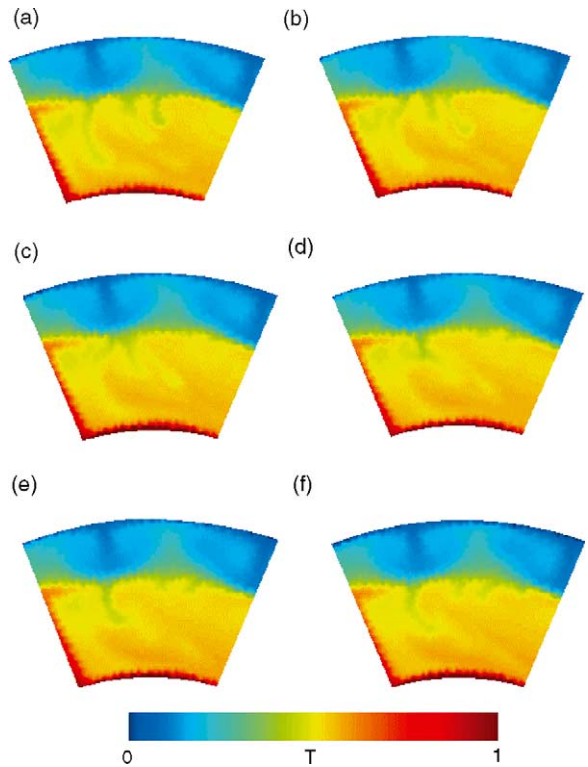


Fig. 8. Development of a long-living slab-like structure in the model (o) (see Table 1). Plots of temperature field extend from the surface to the core–mantle boundary. Time difference between the panels is 20 Myr.

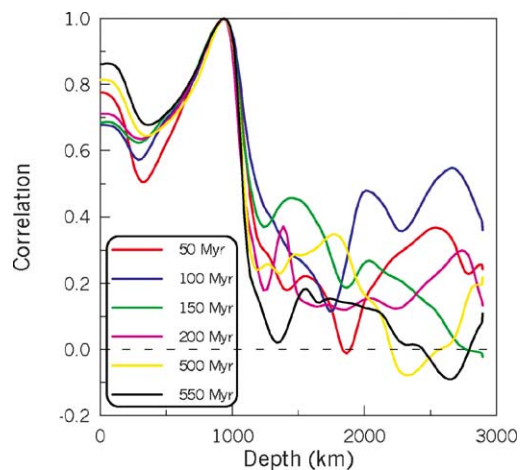


Fig. 9. Autocorrelation function of the temperature distribution at a depth of 950 km and the temperature distribution in the whole mantle plotted for six time intervals.

of hundreds of million years, contrary to the shorter living downwelling structure shown in Fig. 7.

The vertical coherence of upper and lower layer structures on a global scale is demonstrated in Fig. 9 by means of autocorrelation of temperature field. Here the correlation of the temperature distribution at a depth of 950 km (e.g. just above the boundary between the two layers) with the temperature distribution in the whole mantle is shown for six time intervals. The maximum correlation is of course reached at a depth of 950 km, since the layer perfectly correlates with itself. The high correlation is obtained throughout the whole upper layer (from the surface down to the 1000 km), because the upper layer convective features (upwellings and downwellings) are more or less vertical. The correlation in the lower layer is of course substantially lower—the vertical coherence between the separately convecting layers is not perfect. In some time intervals, however, even the correlation in some parts of the lower layer is rather high (100 Myr or 150 Myr—blue and green lines) thus indicating that a thermal coupling mechanism plays an important role.

4. Conclusions

The results of our study indicate that under certain conditions the density contrast of 2–3% is able to prevent the mass exchange between the layers for a substantially long time period. This is only valid if the heat sources located in the lower layer are not too strong and the effect of adiabatic heating/cooling is included. The increase of viscosity with depth may be a stabilizing factor. In the case of the two tested models with radially variable viscosity (models B and C), a density contrast of 2% is sufficient to maintain the layered convection on a time scale of ~ 1000 Myr. However, a somewhat higher density contrast ($\sim 3\%$) is needed to keep the amplitudes of the boundary topography small. The density contrast of 3% would be still rather high from the seismological or mineralogical point of view but as was already pointed out by Kellogg et al. (1999), the actual density contrast across the interface is lower because the compositional and thermal effects of a boundary layer at the 1000 km interface to density cancel out. The excess compositional density of 3% is partially compensated by the thermal effect and, thus, the net density difference between the layers is

only about 1%. The question arises, whether such a low density contrast at a depth of 1000 km could be seismically detectable.

In the model with the average temperature- and depth-dependent viscosity, where the low viscosity channel develops around the 1000 km interface, the thermal coupling mechanism is able to generate slab-like, seemingly continuous cold downwelling structures extending deep into the lower layer. Such thermally coupled ‘slabs’ develop in a relatively short time of about 40 Myr. In some parts of the mantle lower layer downwellings connected with upper layer slabs remain stable on time scales of hundreds of million years.

Acknowledgements

Discussions with Ondřej Čadek, Arie van den Berg and Dave Yuen are gratefully acknowledged. This work was supported by the research projects GAČR 205/01/D046 and 205/02/1306, GAUK 230/2002/B-GEO/MFF, 238/2001/B-GEO/MFF and DG MSM 113200004.

References

- Anderson, D.L., 2001. Top-down tectonics? *Science* 293, 2016–2018.
- Anderson, D.L., 2002. The case of irreversible chemical stratification. *Int. Geol. Rev.* 44, 97–116.
- Bijwaard, H., Spakman, W., Engdahl, E.R., 1998. Closing the gap between regional and global travel time tomography. *J. Geophys. Res.* 103, 30055–30078.
- Christensen, U., Yuen, D.A., 1984. The interaction of a subducting lithospheric slab with a chemical or phase boundary. *J. Geophys. Res.* 89, 4389–4402.
- Čížková, H., Čadek, O., 1997. Effect of a viscosity interface at 1000 km depth on mantle convection. *Studia Geoph. et Geod.* 41, 297–306.
- Čížková, H., Čadek, O., van den Berg, A., 1999. Can lower mantle slab-like seismic anomalies be explained by thermal coupling between the upper and lower mantles? *Geophys. Res. Lett.* 26, 1501–1504.
- Coltice, N., Ricard, Y., 1999. Geochemical observations and one layer mantle convection. *Earth Planet. Sci. Lett.* 174, 125.
- Cserepes, L., Rabinowicz, M., Rosemberg-Borot, C., 1988. Three-dimensional infinite Prandtl number convection in one and two layers with implications for the earth’s gravity field. *J. Geophys. Res.* 93, 12009–12025.

- Cserepes, L., Yuen, D.A., 1997. Dynamical consequences of mid-mantle viscosity stratification on mantle flow with an endothermic phase transition. *Geophys. Res. Lett.* 24, 181–184.
- Davaille, A., 1999. Simultaneous generation of hotspots and superswells by convection in a heterogeneous planetary mantle. *Nature* 402, 756–760.
- Hofmann, A.W., 1997. Mantle geochemistry: the message from oceanic volcanism. *Nature* 385, 219–229.
- Kawakatsu, H., Niu, F., 1994. Seismic evidence for a 920 km discontinuity in the mantle. *Nature* 371, 301–305.
- Kellogg, L.H., Hager, B.H., van der Hilst, R.D., 1999. Compositional stratification in the deep mantle. *Science* 283, 1881–1884.
- Mambole, A., Fleitout, L., in press. Petrological layering induced by an endothermic phase transition in the earth. *Geophys. Res. Lett.* 29 (22).
- Matyska, C., Yuen, D.A., 2002. Bullen's parameter η : a link between seismology and geodynamical modelling. *Earth Planet. Sci. Lett.* 198, 471–483.
- Mitrovica, J., Forte, A., 2002. On the radial profile of mantle viscosity. In: Mitrovica, J.X., Vermeersen, B.L.A. (Eds.), *Ice Sheets, Sea Level and the Dynamic Earth*, American Geophysical Union, pp. 257–273.
- Montagner, J.P., Guillot, L., 2000. Seismic anisotropy in the earth mantle. In: Boschi, E., et al. (Eds.), *Problems in Geophysics for the New Millennium*, Editrice Compositori, Bologna, Italy, pp. 218–253.
- Ricard, Y., Wuming, B., 1991. Inferring the viscosity and 3D density structure of the mantle from geoid, topography and plate velocities. *Geophys. J. Int.* 105, 561–571.
- Richter, F., McKenzie, D., 1981. On some consequences and possible causes of layered mantle convection. *J. Geophys. Res.* 86, 6133–6142.
- Schmus, W.R.V., 1995. Natural radioactivity of the crust and mantle. In: Ahrens, T.J. (Ed.), *Global Earth Physics, A Handbook of Physical Constants*, American Geophysical Union, Washington, USA, pp. 283–291.
- Tackley, P., 2000. Mantle convection and plate tectonics: toward and integrated physical and chemical theory. *Science* 288, 2002–2007.
- Turcotte, D.L., Paul, D., White, W.M., 2001. Thorium–uranium systematics require layered mantle convection. *J. Geophys. Res.* 106, 4265–4276.
- van der Hilst, R.D., Widiyantoro, S., Engdahl, E.R., 1997. Evidence for deep mantle circulation from global tomography. *Nature* 386, 578–584.
- Wen, L., Anderson, D.L., 1997. Layered mantle convection: a model for geoid and topography. *Earth Planet. Sci. Lett.* 146, 367–377.